Electronic structure of $KHgC_4$ and related materials

N. A. W. Holzwarth, Qingsheng Wang, and S. D. Had
Department of Physics, Wake Forest University, Winston-Salem, North Carolina 27109
(Received 22 February 1988)

We report the results of self-consistent calculations of the electronic structure of the ternary graphite intercalation compound $KHgC_4$ and of the structurally related amalgam material $NaHg_2$. Using the local-density approximation and mixed-basis pseudopotential calculational techniques, we are able to evaluate the energy bands, the densities of states, and the valence charge distributions for these materials. In contrast to other graphite donor intercalation compounds, we find that for $KHgC_4$ the intercalate layer retains a significant carrier concentration. The amalgam bands are aligned within the complex of the graphite π bands. The bottom of the Hg 6*s* band lies 2.8 eV above the bottom of the graphite π bands and the bottom of the Hg 6*p* bands lie a few tenths of an eV above the degeneracy point of the graphite π bands. A very rough estimate is that the conduction electrons consist of 1.5 electrons associated with the amalgam layer and 0.5 electrons associated with the graphite π bands for each $K_2Hg_2C_8$ unit cell. Our results for $KHgC_4$ are consistent with some of the experimental results described in the literature.

I. INTRODUCTION

The ternary graphite intercalation compound $KHgC_4$ has been studied by a number of experimental techniques.[1-9] In contrast to many other donor compounds, the metallic properties of this material are thought to be due to charge carriers in the intercalant layers as well as in the graphite π bands. There has been some theoretical work[10] on the second-stage material $KHgC_8$.

In this paper, we report the results of a self-consistent calculation of the electronic structure of $KHgC_4$ and of the structurally related pure-amalgam material $NaHg_2$. We use the local-density approximation[11,12] and mixed-basis pseudopotential methods of calculation.[13] The paper is divided into the following sections. In Sec. II, the calculational details are presented. In Sec. III, the results for the electronic structure of $NaHg_2$ are presented. The results for the electronic structure of $KHgC_4$ are presented in Sec. IV. Discussion and conclusions are given in Sec. V.

II. METHODS OF CALCULATION

A. Band structures

Self-consistent, first-principles band-structure calculations were carried out in the framework of local-density theory[11] in the local-density approximation[12] using mixed-basis pseudopotential techniques.[13-17]

The details of this calculation are similar to that described in our earlier work on the electronic structure of graphite,[18] with the following changes. The functional form of the pseudopotential was that of Kerker,[15] modified to include relativistic effects other than that of the spin-orbit interaction[16,17] and to include the exchange-correlation effects of the approximate core density.[13] The pseudopotential radii were chosen to be 1.4, 2.5, 4.0, and 3.1 bohrs for C, Hg, K, and Na, respectively. This choice enabled us to achieve reasonable basis-set completeness and reciprocal-lattice sum convergence by including all plane waves for $|\mathbf{k}+\mathbf{G}| \leq 3$ Ry and carrying out all reciprocal space sums for $|\mathbf{k}+\mathbf{G}| \leq 25$ Ry.

The matrix elements of the Hamiltonian involving the nonlocal (*l*-dependent) contributions to the pseudopotential[13] were evaluated using a separable form similar to that described in a previous work.[18] However, the specific separable form was based on a Gaussian quadrature approximation to the plane-wave matrix element of the nonlocal pseudopotential $\delta\Phi_{\tau l}(r)$ of site τ and angular momentum *l*:

$$V_{\mathrm{NL}}(\mathbf{k}+\mathbf{G},\mathbf{k}+\mathbf{G}')=\sum_{\tau,l,M,n} A_{\tau ln} f_{\tau l\mathrm{Mn}}(\mathbf{k}+\mathbf{G}) \times f^{*}_{\tau l\mathrm{Mn}}(\mathbf{k}+\mathbf{G}') , \quad (1)$$

where

$$f_{\tau l\mathrm{Mn}}(\mathbf{k}+\mathbf{G})=\exp(-i\mathbf{G}\cdot\boldsymbol{\tau})Y_{lM}\hat{u}_{\mathbf{k}+\mathbf{G}}j_l(|\mathbf{k}+\mathbf{G}|r_n) ,$$

$\hat{u}_{\mathbf{k}+\mathbf{G}}$ denotes a unit vector along $\mathbf{k}+\mathbf{G}$, and

$$A_{\tau ln}=\frac{(4\pi)^2}{\Omega}\frac{r_{\tau l}}{2}r_n^2\delta\Phi_{\tau l}(r_n)W_n .$$

In this expression, W_n and r_n denote, respectively, the Gaussian weights and abscissas for evaluating the plane-wave matrix element of $\delta\Phi_{\tau l}(r)$ in the range $0<r<r_{\tau l}$. Typically, the order of the Gaussian quadrature could be chosen to be 10–30 for high accuracy. In the above expression, $\mathbf{k}$ denotes the wave vector, $\mathbf{G}$ represents a reciprocal-lattice vector, and Ω is the unit-cell volume. We believe this method to be quite efficient and generally applicable to mixed-basis pseudopotential calculations.

B. Densities of states

One of the challenges of performing a self-consistent calculation of a multicomponent metallic system is adequate **k**-space sampling and calculation of the density of states. Because of the proximity of a large number of bands in these materials, methods based on local interpolation[19] are likely to yield spurious results. The method of Gilat and Raubenheimer[20,21] based on extrapolation using band energies and their gradients is preferable.

In order to implement the Gilat-Raubenheimer scheme for our materials, we used the parallelepiped form of the unit cell formed from the three translation vectors $\mathbf{T}_1$, $\mathbf{T}_2$, and $\mathbf{T}_3$. Each translation vector $\mathbf{T}_i$ was then divided into n_i equal segments to form $n_1 \times n_2 \times n_3$ small parallelepipeds. For both the density of states and the charge-density evaluations, the energy bands and their gradients were evaluated at the midpoints of each nonequivalent small parallelepiped. For $KHgC_4$, n_1, n_2, and n_3 were chosen to be 6, 6, and 2, respectively, corresponding to 21 nonequivalent **k** points. For $NaHg_2$, they were chosen to be 6, 6, and 6, corresponding to 36 nonequivalent **k** points. We estimate that these choices yield density-of-state results which have an error of at most 20%. The parallelepiped geometry can be mapped into a rectangular solid geometry in order to use the general density-of-state formulation of Gilat and Kam.[21]

The energy-band gradients were calculated in two steps. First the energy bands were calculated as described in Sec. II A, and the eigenvalues and eigenvectors were stored in a file. The gradients were then calculated in a separate program based on the Feynman-Hellman theorem[22] modified for contributions from the nonorthogonality of the mixed-basis wave functions.[13] For each wave vector **k**, the mixed-basis eigenvalue problem can be written in the generalized form[13]

$$(H - ES)\Lambda = 0 , \tag{2}$$

where H is the Hamiltonian, S is the overlap matrix, E is the energy-band eigenvalue, and Λ is the corresponding eigenvector of plane wave and linear combination of atomic orbital (LCAO) coefficients. In order to calculate the gradients with respect to **k**, it is convenient to express these quantities in terms of a plane-wave basis. For this purpose, there exists a rectangular matrix U such that

$$H = U^{\dagger} H_P U$$

and

$$S = U^{\dagger} U , \tag{3}$$

where H_P denotes the Hamiltonian evaluated in the plane-wave basis. In these terms, the gradient of each energy band can be evaluated according to

$$\nabla E = \Lambda^{\dagger} U^{\dagger} \nabla H_P U \Lambda + \Lambda^{\dagger} \nabla U^{\dagger} (H_P - E) U \Lambda + \Lambda^{\dagger} U^{\dagger} (H_P - E) \nabla U \Lambda . \tag{4}$$

In the above expression, ∇ denotes the gradient with respect to **k**. Once the energy-band gradients were calculated for all of the bands at each of the midpoint wave vectors, they were used for calculating the density of states according to the Gilat-Raubenheimer-Kam[20,21] algorithm.

For some of the calculations in this study it was important to calculate the partial densities of states. For this, we took advantage of the layer geometry and used the charge within a layer associated with each state as a weight factor, neglecting its gradient contribution.[21] For the calculations of the partial density of Hg states presented in Sec. IV, the layer was centered in the Hg plane and its thickness was taken to be 2.84 Å, which is the distance between Hg atoms in a layer.

III. ELECTRONIC STRUCTURE OF $NaHg_2$

The sodium-amalgam compound $NaHg_2$ has intriguing structural similarities to the graphite intercalation compound $KHgC_4$. It forms in the hexagonal AlB_2 structure having $P3m1$ (D_{3d}^3) symmetry with lattice constants $a = 5.0290$ Å and $c = 3.2304$ Å.[23] The hexagonal arrangement of Hg atoms in a layer of this compound is the same as the hexagonal arrangement of Hg atoms in $KHgC_4$ except for a 2% dilation of the lattice constant a. The arrangement of the alkali-metal atoms with respect to the Hg hexagons is also similar to that in the intercalant layer of $KHgC_4$. On the other hand, $NaHg_2$ has a substantial amount of interlayer bonding between Hg atoms; the nearest-neighbor distance between the A-A stacked Hg layers being only 10% larger than the nearest-neighbor Hg distance within a layer. Another difference is that in $NaHg_2$, each layer of Na is shared by two layers of Hg so that there are half as many alkali-metal atoms for each Hg atom as in the intercalation compound.

The structure of the potassium-amalgam compound KHg_2 has also been determined.[24] Apparently, its structure is similar to that of $NaHg_2$, but the Hg layers are buckled in order to accommodate the larger K atoms. The potassium amalgam compound KHg has also been characterized,[24] but its structure is even more complicated. Hence, for purposes of comparison with the simplest possible structure of alkali-metal-amalgam graphite intercalation compound $KHgC_4$,[6] we chose to study the electronic structure of $NaHg_2$.

We have determined the electronic structure of $NaHg_2$ using the methods described in Sec. II. The pseudopotential approximation is ideal for Na and introduces negligible errors. However, for Hg some limitations should be noted. Not included in this calculation are the Hg 5d states which lie approximately 3–5 eV below the valence bands. Also not well determined are the Hg 5f states which are unoccupied and lie approximately 0.5 eV above the 6p states in atomic Hg. Since the pseudopotential represents the relativistic spin-averaged interaction, the splitting between the Hg 6s and 6p states is well determined. However, the spin-orbit interaction has not been included. In atomic Hg this results in a further splitting of the Hg 6p states of approximately 1 eV which, although not negligible, is less than the bandwidths of this material.

The valence-band structure and density of states of $NaHg_2$ are shown in Fig. 1, where the zero of energy is taken to be the Fermi level. The lowest valence bands of this material are due to the Hg 6*s* states. These bands are nearly completely filled except for a relatively small region centered at the *A* point of the Brillouin zone. The Hg 6*p* states lie at higher energy and are partially filled. Due to the strong interlayer interaction, the band dispersion along the *c* axis is comparable to that within the *a* plane. Because of the hexagonal structure, the Hg $6p\sigma$ states and π states form separate bands, the bottom of π band lying 1.0 eV lower than that of the σ band. The Hg $6p\pi$ bands overlap with the 6*s* bands in the vicinity of the *A* plane of the Brillouin zone.

The density of states shows two main structures. The lower-energy structure, lying between -8 eV and -4 eV, is mainly due to states of Hg 6*s* character. The higher-energy structure, lying between -1 eV and $+3$ eV, is mainly due to states of Hg 6*p* character. The fermi surface has three sheets. One is due to Hg $6p\sigma$ contributions having a band minimum at the *K* point of the Brillouin zone. A second sheet is due to Hg $6p\pi$ contributions having a band minimum at the *A* point. The third sheet is due to a small, nearly spherical, hole contribution from the Hg $6s\sigma^*$ band centered at the *A* point. The value of the Fermi-level density of states is 1.3 states eV^{-1} $(NaHg_2$ unit$)^{-1}$.

The Na 3*s* states contribute throughout the band structure where allowed by symmetry. Because of the extended range of the Na 3*s* wave function, it is difficult to quantify its contribution. However, based on the magnitude of the Na 3*s* coefficient in our mixed-basis representation, a large contributions occur at the Γ point at the bottom of the Hg $6s\sigma$ band at -8.5 eV and at the *A* point at the bottom of the Hg $6p\pi$ band at -2.0 eV. A more obvious contribution of Na is to add a valence electron in each unit cell of the system. In a simple rigid-band picture, removing the Na electron would lower the Fermi level by 1.2 eV. This would remove most of the Hg 6*p* occupancy except for a small contribution of states near the bottom of the π band and substantially lower the Fermi-level density of states. In the graphite intercalation compound $KHgC_4$, there are twice as many alkali-metal atoms per Hg atom as there are in $NaHg_2$. In a simple rigid-band picture, adding a second Na electron to each unit cell (Na_2Hg_2) would raise the Fermi level by 0.8 eV, increasing the Hg 6*p* occupancy and decreasing the Fermi-level density of states.

Contour plots of valence pseudodensity[25] for $NaHg_2$ in three different planes are shown in Fig. 2. The peak valence pseudodensity of 0.18 electrons/$Å^3$ occurs in the Hg planes along the Hg—Hg bond direction. The peak position is determined by the last peak in the Hg 6*s* valence wave function which occurs at 80% of the midpoint of the Hg—Hg bond. A somewhat lower peak density occurs along the Hg—Hg bond direction along the *c* axis. The density in the Na plane peaks at 0.13 electrons/$Å^3$ and the shape of the contours reflect the projections of Hg in the parallel planes.

IV. ELECTRONIC STRUCTURE OF $KHgC_4$

The crystal structure of $KHgC_4$ has been determined from x-ray diffraction by Lagrange, Makrini, and Herold.[6] The layer sequence of this compound is C-K-Hg-K-C-K-Hg-K-C-$\cdots$. The potassium layers form a triangular lattice as in the binary compound C_8K. In the simplest interpretation of the x-ray results,[6] the Hg layers form a plane hexagonal lattice twice as big as the hexagonal graphite layers. In the present work, we consider only this simple planar structure for the Hg layers. Furthermore, to reduce the computation to manageable size, we simplified the stacking sequence of the K-Hg-K registry with respect to the graphite lattice. The x-ray analysis suggests that $KHgC_4$ has a stacking sequence of $A\alpha A\beta A\gamma A\delta A\alpha\ldots$.[6] By simplifying this stacking sequence to $A\alpha A\beta A\alpha A\beta\ldots$, the unit cell is reduced, by a factor of four, to 12 atoms (eight C atoms, two Hg

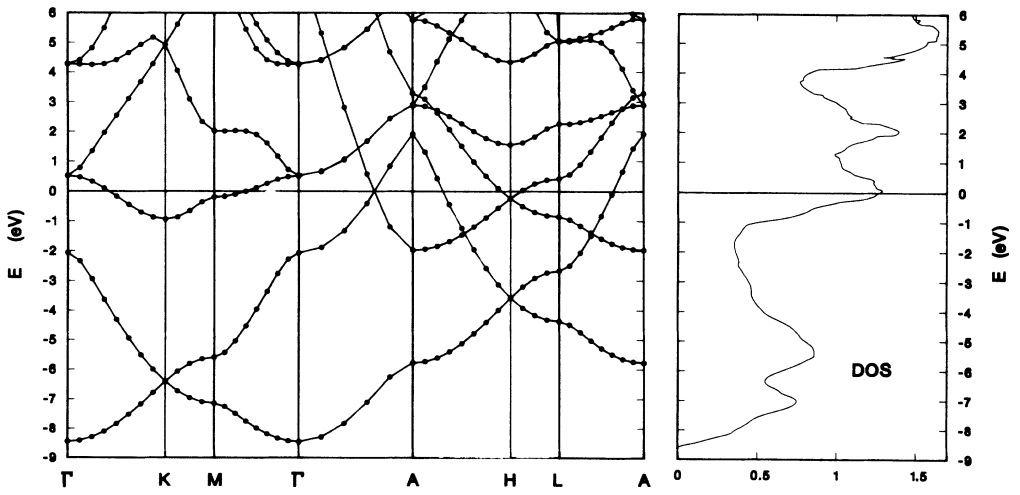

FIG. 1. Band structure and density of states for $NaHg_2$. Bands are shown along various directions in the hexagonal Brillouin zone. The density of states is given in units of states eV^{-1} $(NaHg_2$ unit$)^{-1}$. The zero of energy is chosen to be the Fermi level.

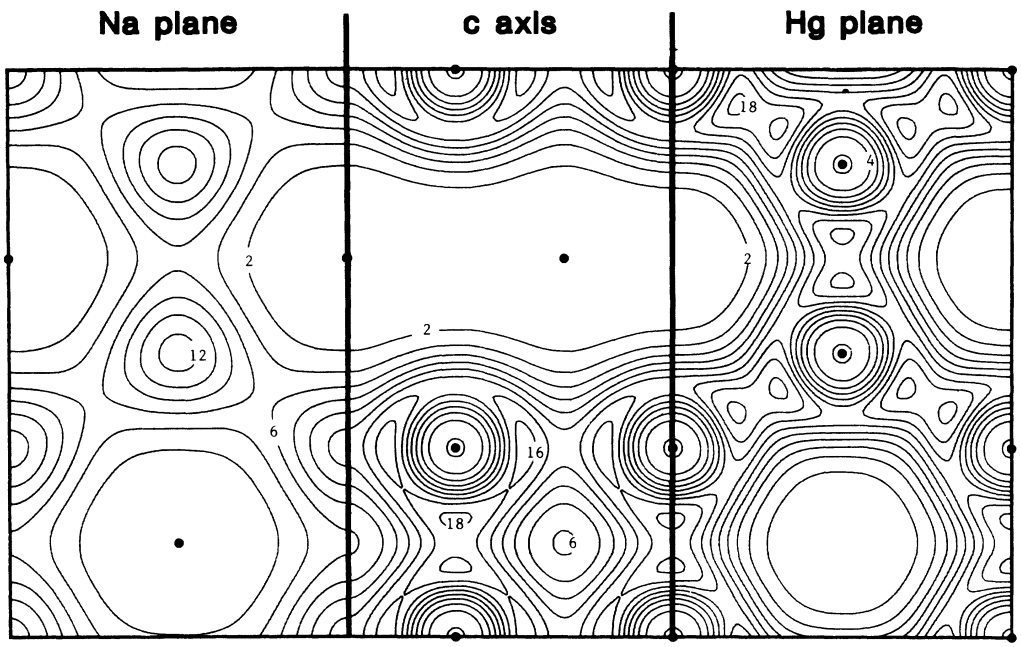

FIG. 2. Charge-density contours for $NaHg_2$ shown in three connected planes. Left panel, in a plane containing only Na atoms; central panel, in a plane containing the c axis and passing through Hg and Na atoms; right panel, in a plane containing only Hg atoms in a hexagonal structure. Atomic positions are denoted by solid circles. Contour labels are in units of 0.01 electrons/Å^3. Contour levels are equally spaced in intervals of 0.02 electrons/Å^3.

atoms, and two K atoms) while the nearest layer geometry is preserved. This structure has eightfold symmetry, including an inversion center at the center of a C—C bond. A similar simplification in the treatment of the electronic structure of KC_8 by Tatar and Rabii[26] yielded results consistent with calculations for the actual structure by DiVicenzo and Rabii.[27] Furthermore, neutron scattering results by Kamitakahara and co-workers[5] suggest that the stacking sequence $A\alpha A\beta A\alpha A\beta\ldots$ may be present, at least in some samples of $KHgC_4$.

A diagram of the simplified unit cell is shown in Fig. 3. The lattice parameters determined by the x-ray analysis[6] are $c=10.16$ Å for the c axis and $a=|\mathbf{T}_1-\mathbf{T}_2|=4.92$ Å for the a axis. From the translation vectors defined in Fig. 3, the corresponding reciprocal-lattice vectors $\mathbf{G}_1$, $\mathbf{G}_2$, and $\mathbf{G}_3$ were formed. For analysis of the band dispersions, the electronic structure was plotted along the following directions (see Fig. 4):

$$\begin{aligned}
&x(\mathbf{G}_1-\mathbf{G}_2) \text{ for } 0\le x\le\tfrac{1}{3}, \text{ labeled } \Gamma\text{-}K\ ,\\
&x(\mathbf{G}_1-\mathbf{G}_2) \text{ for } \tfrac{1}{3}\le x\le\tfrac{1}{2}, \text{ labeled } K\text{-}M\ ,\\
&\mathbf{G}_1-\mathbf{G}_2+x\mathbf{G}_3 \text{ for } 0\le x\le\tfrac{1}{2}, \text{ labeled } M\text{-}M'\ , \qquad (5)\\
&x(\mathbf{G}_1+\mathbf{G}_2+\mathbf{G}_3) \text{ for } \tfrac{1}{2}\ge x\ge 0, \text{ labeled } M'\text{-}\Gamma\ ,\\
&x\mathbf{G}_3 \text{ for } 0\le x\le\tfrac{1}{2}, \text{ labeled } \Gamma\text{-}A\ .
\end{aligned}$$

For convenience, we have labeled the Brillouin-zone directions for the $KHgC_4$ structure with the same symbols used for similar directions in the hexagonal Brillouin zone of $NaHg_2$. We have used the symbol M' to denote both $(\mathbf{G}_1-\mathbf{G}_2+\mathbf{G}_3/2)$ and $(\mathbf{G}_1+\mathbf{G}_2+\mathbf{G}_3/2)$, which are equivalent in this structure.

Our treatment of Hg in $KHgC_4$ is subject to the same limitations described in our treatment of $NaHg_2$. We expect that our semirelativistic pseudopotential treatment of C and K is quite accurate. X-ray photoemission measurements[1] for $KHgC_4$ have observed the Hg $5d$ core

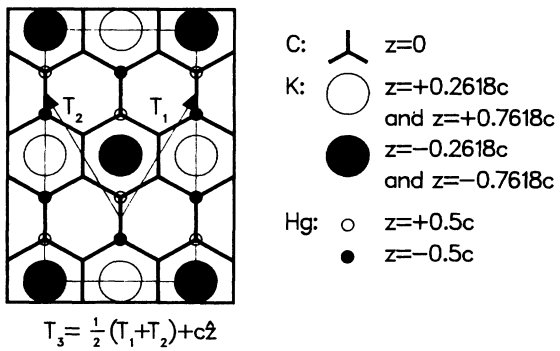

FIG. 3. Diagram of the c-axis projection of the $A\alpha A\beta A\alpha A\beta\ldots$ unit cell for $KHgC_4$ used in this study. $\mathbf{T}_1$ and $\mathbf{T}_2$ denote the layer translation vectors shown originating at the inversion center of the unit cell in the $z=0$ layer. Layer positions are indicated on the right-hand side of the diagram in terms of the c-axis repeat distance as determined in Ref. 6. The thin rectangle in the diagram outlines regions shown in the contour plots of Figs. 5, 8, 9, and 10.

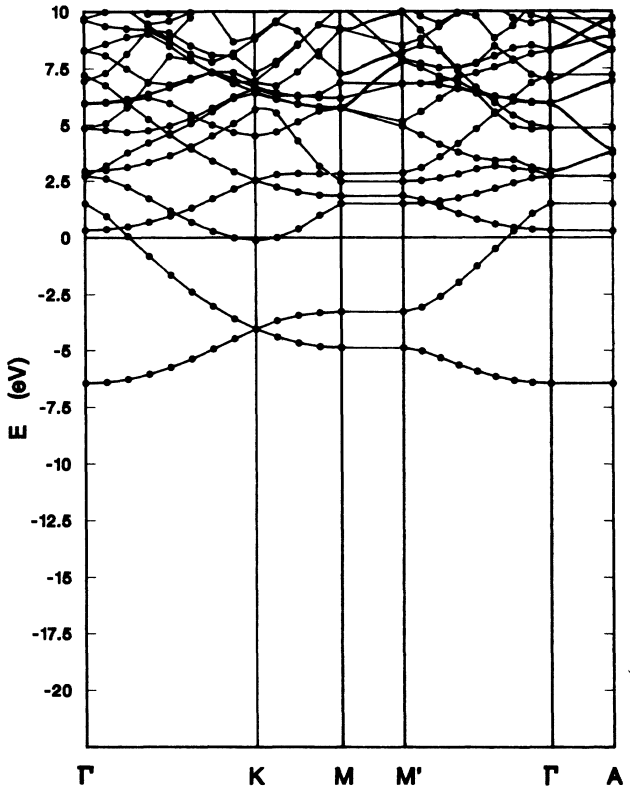

FIG. 4. Self-consistent band structure of a hypothetical material having only Hg atoms in the $KHgC_4$ structure. The zero of energy is the Fermi level corresponding to two valence electrons for each Hg atom. The Brillouin-zone labels are as described in Eq. (5).

states at 8–10 eV below the Fermi level and K $3p$ core states at 18–20 eV below the Fermi level. These core levels overlap with the graphite valence states, but are not treated in our calculations.

In preparation for the study of the intercalation compound, we first studied the self-consistent electronic structure of a hypothetical material having only Hg atoms in the $KHgC_4$ structure. The band structure for this hypothetical Hg material is shown in Fig. 4, where the zero of energy is the Fermi level, corresponding to two valence electrons per Hg atom (four valence electrons per unit cell.) The similarities between the bands of this hypothetical Hg and that of $NaHg_2$ shown in Fig. 1 are apparent. One major difference is that the strong c-axis dispersion in $NaHg_2$ is missing in the hypothetical Hg, where the occupied bands are essentially dispersionless along the c axis. Another difference is that $NaHg_2$ has an additional electron per unit cell compared with the hypothetical Hg. The lowest-energy bands in the hypothetical Hg are those derived from the Hg $6s$ states which are nearly filled except for a small cylindrical region near the Γ-A axis. The Hg $6p\pi$ states have minima at Γ and A just above the Fermi level. This structure corresponds to the π bands in $NaHg_2$ centered at the A point of that Brillouin zone. The Hg $6p\sigma$ states in hypothetical Hg form a band having a minimum at the K point, very slightly below the Fermi level. The analogous band in $NaHg_2$ also has a minimum at the K point of that structure. A few eV above the Fermi level, a large number of Hg bands are shown. This qualitative feature seems to be characteristic of Hg in a variety of crystal structures.[28] A contour plot of the valence charge density for this material is shown in Fig. 5. There is a very close similarity in the valence charge density in the Hg plane for this material and that of $NaHg_2$ shown in Fig. 2; the density of $NaHg_2$ having higher peaks than that of hypothetical Hg in this plane.

The band structure and density of states for $KHgC_4$ are shown in Fig. 6. To a first approximation, the results can be described as a superposition of graphite and Hg bands having relatively weak hybridization. The graphite bands of $KHgC_4$ are very similar to those of KC_8.[26,27,29] The Fermi level lies 21.9 eV above the bottom of the C valence bands, similar to that found in self-consistent treatments of other first-stage donor graphite intercalation compounds.[26,30,31]

Within the complex of graphite bands, it is possible to pick out the Hg bands of $KHgC_4$ which are very similar to those of the hypothetical Hg material shown in Fig. 4. Some of the Hg band extrema are compared in Table I. From this table it is apparent that except for small relative shifts of the bands, the major difference between the materials is that in the hypothetical Hg material, the Hg $6p$ bands are essentially unoccupied, while in $KHgC_4$ the Fermi level lies approximately 1 eV above the Hg $6p$ minima. From this point of view, the Hg layers of $KHgC_4$ are negatively charged, similarly to their charging in $NaHg_2$.

Another important consideration is the relative alignment of the Hg bands with those of graphite in this ma-

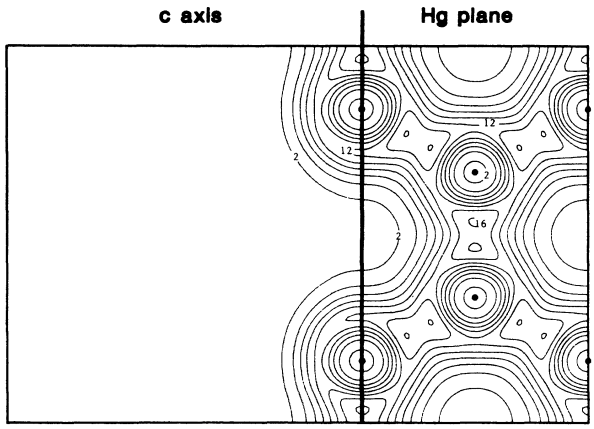

FIG. 5. Charge-density contours for hypothetical Hg shown in two connected planes. Left panel, in a plane containing the c axis and passing through Hg—Hg bonds; right panel, in a plane containing a hexagonal Hg layer. Atomic positions are denoted by solid circles. Contour labels are in units of 0.01 electrons/Å; contour levels are equally spaced at intervals of 0.02 electrons/Å^3.

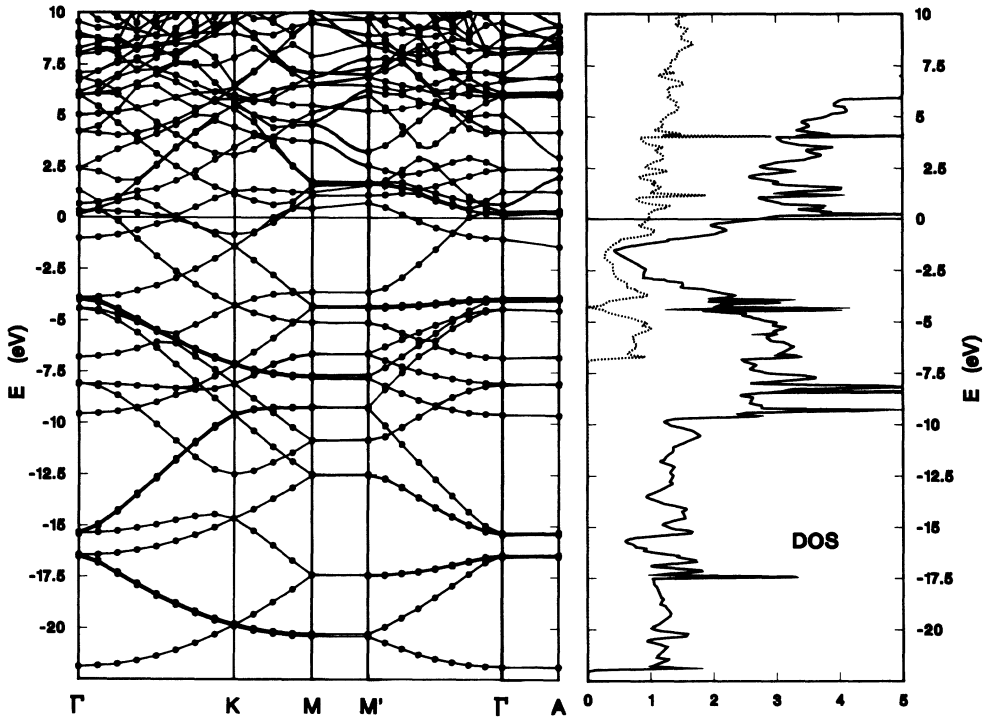

FIG. 6. Band structure and density of states for $KHgC_4$. The Brillouin-zone labels are as described in Eq. (5). The zero of energy is the Fermi level corresponding to 38 valence electrons per unit cell. The density of states (solid line) is given in units of states eV^{-1} $(K_2Hg_2C_4$ unit$)^{-1}$. The partial density of Hg states are indicated in the same graph with a dotted line.

terial; specifically those of the graphite π bands. Table I also lists some of the band extrema of the graphite π bands found in $KHgC_4$. In graphite, the Fermi level lies near the band-degeneracy point at the K point in the Brillouin zone. In $KHgC_4$, this feature is also located at the K point in its Brillouin zone and is found below the Fermi level at -1.4 eV, corresponding to substantial charge transfer to the graphite π bands. This shift of the Fermi level with respect to that of graphite is slightly less than that found for KC_8.[26] Comparing the graphite π band extrema with those of Hg, we find that the Hg bands lie within the graphite π band complex. The bottom of the Hg 6s band lies 2.8 eV above the bottom of the graphite π and the bottom of the Hg 6p bands lie a few tenths of an electron volt above the graphite π degeneracy point at K.

Because of the large spatial extent of the K atom, the contribution of K states to $KHgC_4$ is difficult to quantify. However, based on the amplitude of the K 4s localized orbital in our mixed-basis wave functions, we are able to identify states which have substantial K 4s character.

TABLE I. Comparison of band energies for $KHgC_4$ and hypothetical Hg material. (Band energies measured in eV with respect to Fermi level of each material.)

Band type	$KHgC_4$	Hg in $KHgC_4$ structure
Hg6$s\sigma$ (band minimum at Γ)	-6.8	-6.4
6$s\sigma^*$ (band maximum at Γ)	$+1.3$	$+1.5$
Hg6$p\pi$ (band minimum at Γ)	-1.0	$+0.3$
6$p\sigma$ (band minimum at K)	-0.8	-0.1
C 2$p\pi$ (band minimum at Γ)	-9.6	
(bands at Γ; derived from	-4.0	
M point in graphite)	-3.9	
(band degeneracy point at K)	-1.4	
(bands at Γ; derived from	$+0.2$	
M point in graphite)	$+0.3$	

TABLE II. Band energies (in eV) $KHgC_4$ for states having significant K 4s amplitude in their mixed-basis eigenvectors (including states at Γ and A with $E \leq 5.0$ eV).

Description of state	Band energy at Γ	Band energy at A
C $2p\pi$+K 4s (bonding)	−9.6	−9.6
Hg $6s\sigma$+K 4s (bonding)	−6.8	−6.8
Hg $6p\pi$+K 4s (bonding)	−1.0	−1.4
C $2p\pi$+K 4s (bonding)	+0.2	+0.4
	+0.3	
Hg $6s\sigma$+K 4s (antibonding)	+0.7	+2.0
Hg $6p\pi$+K 4s (antibonding)	+5.0	+3.0

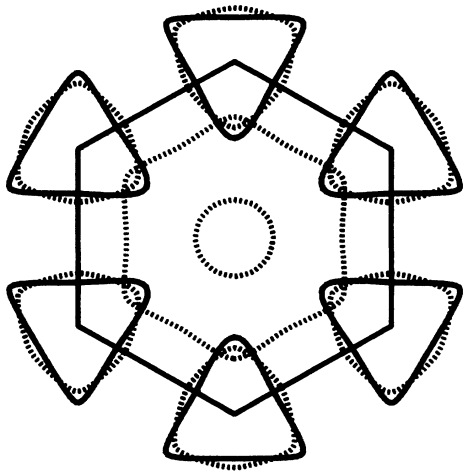

FIG. 7. Very rough guess of Fermi-surface structure of $KHgC_4$ based on band-structure results shown in Fig. 6. The cross sections of the Fermi surfaces are shown in the hexagonal Brillouin zone of the Hg and K layers. Graphite π band contributions are indicated with solid curves; Hg contributions are indicated with dotted curves, including a small hole contribution (Hg 6s) at the zone center, a large electron contribution (Hg $6p\pi$) at the zone center, and an electron contribution (Hg $6p\sigma$) centered at the zone corners. For clarity, we have shown the Fermi surfaces as interpenetrating.

The band energies for these states at the Γ and A points in the Brillouin zone are listed in Table II. The K 4s hybridizes most strongly with the Hg $6p\pi$ states. The bonding combination occurs at −1.0 to −1.4 eV and the antibonding combination occurs at +5.0 to +3.0 eV along Γ-A in the Brillouin zone. The K 4s also hybridizes with the Hg $6s\sigma$ states, resulting in a bonding band at −6.8 eV and an antibonding band at +0.7 to +2.0 eV along Γ-A. Potassium 4s hybridization also occurs with the Hg $6p\sigma$ at −1.2 eV at the K point of the Brillouin zone. Many of these structures are also present in $NaHg_2$. A notable exception is the antibonding combination of the Hg $6s\sigma$ and alkali s state which is shifted in $NaHg_2$ by more than 10 eV above the Fermi level due to strong interlayer Hg interactions. As in KC_8,[26] the K 4s states also interact significantly with the graphite $2p\pi$ bands, forming bonding configurations at the bottom of graphite π at −9.6 eV and at the π bands located a few tenths of an eV above the Fermi level. The latter structure corresponds to the M point π bands in the original graphite Brillouin zone.

The occupied states of $KHgC_4$ are essentially dispersionless along the c axis, which is not surprising due to the very large c-axis lattice parameter. Thus, we would expect the Fermi surfaces to be cylindrical. A very rough guess of the Fermi surface structure, based only on the band structure results shown in Fig. 6 and on the assumption of approximate hexagonal symmetry, is sketched in Fig. 7 in the two-dimensional Brillouin zone of the K-Hg-K layers. This figure indicates the c-axis cross sections of the four main contributions to the Fermi surface. For simplicity, we have shown the various contributions as overlapping, although in a realistic treatment this is not correct. The partially filled graphite π band contributes triangular cross sections centered at the zone corners, similarly to KC_8.[26,29] Also at the zone corners are surfaces due to the partially filled Hg $6p\sigma$ band. At the zone center there is a small cross section due to the Hg 6s holes and a larger cross section due to the partially filled Hg $6p\pi$ band. From a very rough estimate of the areas in each of these cross sections, we can say the following about the charge transfer. The graphite π band and the Hg $6p\sigma$ band each accommodate 0.5 excess electrons. The Hg $6p\pi$ band accommodates 1.1 excess electrons, while the Hg 6s hole surface accounts for a deficit of roughly 0.1 electrons. In this picture, the two excess K electrons per unit cell are distributed with 0.5 electrons in the graphite π band and 1.5 electrons in the amalgam bands. We stress that this distribution is highly speculative since it is sensitive to details of the band structure beyond the accuracy of our calculation. In particular, the effects of spin-orbit interaction, which have not been included in the present analysis, probably shift the Hg 6p bands by a few tenths of an electron.

On the right-hand side of Fig. 6 the total density of states of $KHgC_4$ (solid line) and the partial density of states of the Hg layers (dotted line) are shown. Some of the interesting features of the density of states results are as follows. The bottom of the graphite π band at −9.6 eV marks a general increase in the density of states. The graphite π band degeneracy point at the K point of the Brillouin zone at an energy of −1.4 eV marks a dip in the density of states. The Hg partial density of states has an onset at −6.8 eV and goes to zero at −4.3 eV at the degeneracy point for the Hg $6s\sigma$ point at the K point in the Brillouin zone. There is a peak in the partial density of states of 1.1 states eV^{-1} (unit cell)$^{-1}$ at −0.6 eV due to the onset of the Hg 6p bands, slightly above its value at the Fermi level. This peak is slightly less than the corresponding peak value of the density of states per Hg atom found for $NaHg_2$ shown in Fig. 1.

The total density of states at the Fermi level of this material is 2.7 states eV^{-1} ($K_2Hg_2C_8$ unit)$^{-1}$, or 0.23 states eV^{-1} atom.$^{-1}$ Our partial density-of-states analysis estimates that the Hg contribution to this density of

states is 1.0 states eV^{-1} $(K_2Hg_2C_8$ unit$)^{-1}$.

The integrated charge within the Hg layer can give some indication of the spatial distribution of charge. There are a total of 38 valence electrons in our system. Using the same layer thickness as in the partial density-of-states analysis, we find that the Hg layer contains 4.3 electrons, leaving 33.7 electrons distributed in the C and K layers. One interpretation of this result is that the two electrons available from K are distributed such that the Hg layers receive 0.3 extra negative charges while 1.7 electrons are donated to graphite or remain in a K layer. This result is highly sensitive to the choice of the Hg layer thickness, which we have taken to be equal to the Hg intralayer bond length of 2.84 Å, perhaps too small to adequately take into account the extended Hg $6p\pi$ states. The charge distribution indicated by the Fermi surface analysis above suggests the opposite picture; that a larger portion of the excess charge is associated with the amalgam layer.

In order to get a better idea of the spatial distribution of charge in this material, it is helpful to consider the charge-density contours shown in Figs. 8 and 9. The charge density in the C plane is shown in Fig. 8 in relation to the density along the c axis and in the Hg plane. The area shown in the C and Hg planes is that outlined in the unit-cell diagram of Fig. 3. The C contours look very similar to those found in graphite and other intercalation compounds.[18,26,30] The density in the Hg plane is considerably less; the peak density in the Hg plane of 0.18 electrons/Å^3 is 11 times smaller than the peak density in the C plane of 2.09 electrons/Å^3. In Fig. 9, a higher-resolution plot of the valence pseudocharge density for $KHgC_4$ is shown, using the same contour levels as shown in Figs. 2 and 5 for $NaHg_2$ and hypothetical Hg, respectively. From this figure, it is apparent that the charge density in a Hg plane of $KHgC_4$ is generally smaller, especially along Hg—Hg bond directions than in both $NaHg_2$ and in hypothetical Hg. In order to examine this feature in greater detail, we have evaluated the difference between the density of $KHgC_4$ minus that of hypothetical Hg and plotted the result in Fig. 10. In this higher-resolution plot, we see that charge has been polarized toward the K^+ ions at the expense of charge along the Hg—Hg bonds. This is similar to charge redistribution in the graphite layer studied in other intercalation compounds.[31] Since the charge donation has occurred largely to states of π character which have zero density in the Hg plane, the combination of the electrostatic polarization by the K^+ ions and the charge donation are able to result in a charge deficit in the Hg planes in the difference density plot. In contrast to the situation in the C planes, however, some of the charge donation results in the occupation of Hg $6p\sigma$ states as well as π states. Although we did not specifically study it in this work, the K^+ ions probably also polarize the graphite charge density similarly to the polarization found in other donor intercalation compounds.[31]

V. DISCUSSION AND CONCLUSIONS

An approximate calculation of the electronic structure of the second-stage compound $KHgC_8$ has been carried out by Senbetu, Ikezi, and Umrigar.[10] They carried out a self-consistent calculation for an isolated film of the amalgam K-Hg-K, with results very similar to states of the

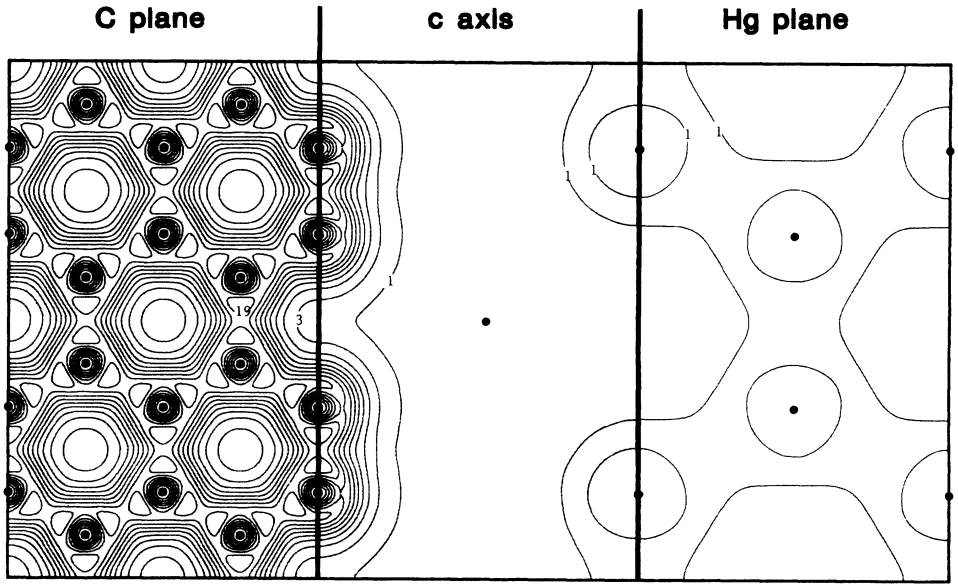

FIG. 8. Contour plot of the valence pseudodensity for $KHgC_4$ shown in three connected planes—a C plane (left panel); a plane containing the c axis and passing through intralayer C—C bonds and Hg—Hg bonds (middle panel); and a Hg plane (right panel). Atomic positions are denoted with solid circles. Contour levels are given in units of 0.1 electrons/Å^3 and are given in uniform intervals of 0.2 electrons/Å^3, starting at 0.1 electrons/Å^3.

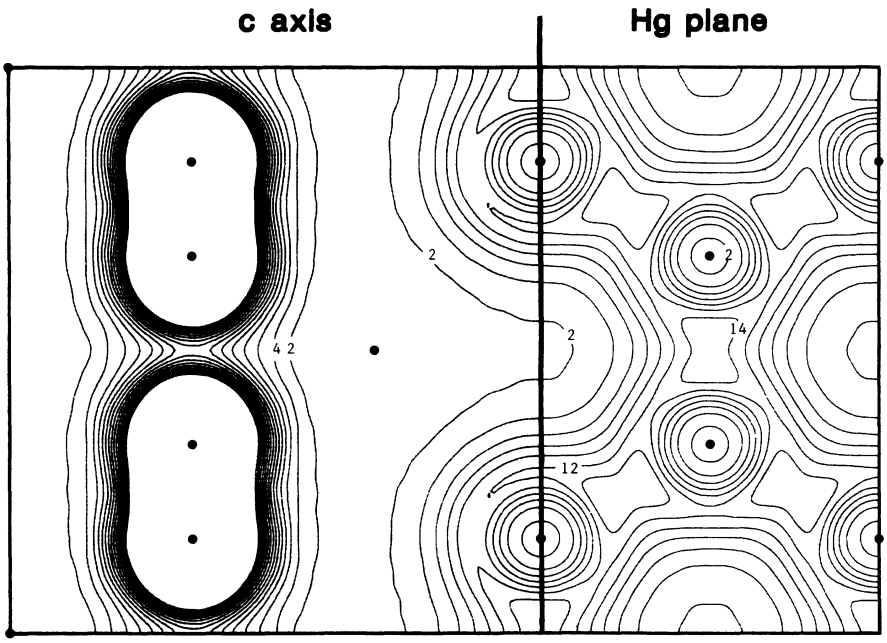

FIG. 9. Higher-resolution contour plot of the valence pseudodensity for $KHgC_4$ shown in two connected planes at closer contour spacings than in Fig. 8. Contour values are in units of 0.01 electrons/Å^3 and are given in uniform intervals of 0.02 electrons/Å^3 except in the high-density region near the C atoms where they are omitted.

hypothetical Hg presented in Fig. 4. However, they were unable to accurately address the question of charge transfer between the graphite and amalgam layers.

Specific-heat measurements for $KHgC_4$ were carried out by Alexander *et al.*[9] Assuming a value of zero for the electron-phonon enhancement factor λ_P, they infer the fermi-level density of states to be 0.40 states eV^{-1} atom^{-1}. Later work by Iye and Tanuma[32] suggested a value of $\lambda_P = 0.38$, which would reduce the Fermi-level density of states inferred from the specific-heat measurements[9] to 0.29 states eV^{-1} atom^{-1}, in good agreement with our calculated result of 0.23 states eV^{-1} atom^{-1}.

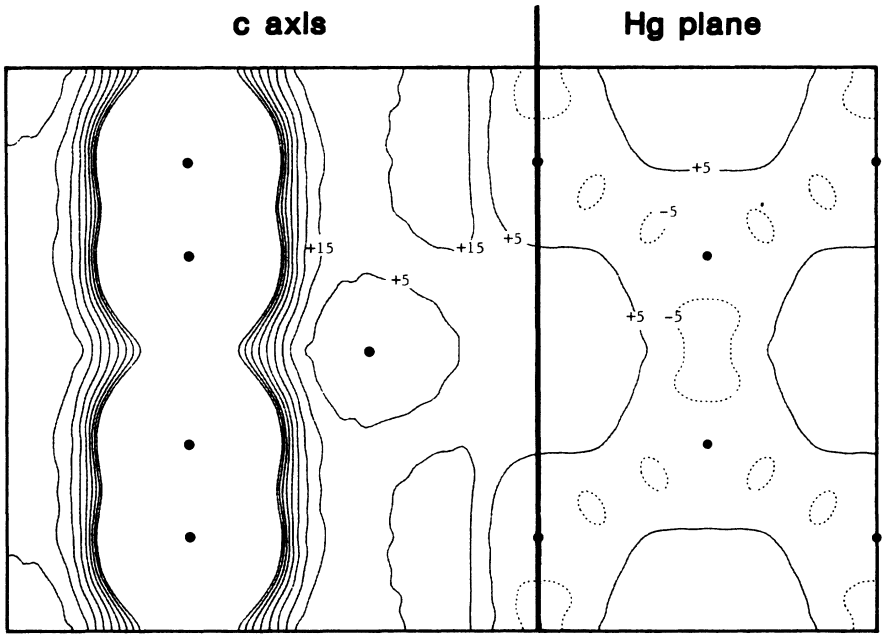

FIG. 10. Contour plot of the difference density of $KHgC_4$ minus that of hypothetical Hg shown in two connected planes as in Figs. 5 and 8. Contour values are in units of 0.001 electrons/Å^3 and are given in intervals of 0.01 electrons/Å^3 starting at -0.005 electrons/Å^3. Contours in the dense region near the C atoms have been omitted. Negative contours, corresponding to lower density in $KHgC_4$ relative to that of hypothetical Hg, are shown with dotted curves.

We can speculate from our density of states as a function of energy (Fig. 6) on the interesting comparison between stages 1 and 2 for this material. It has been suggested[2] that although the Fermi-level density of states for $KHgC_8$ is lower than that of $KHgC_4$,[9] the amalgam contribution to the density of states must be greater for the second-stage material. To a first approximation, one expects the band structure of $KHgC_8$ to be similar to that shown in Fig. 6 with the addition of an extra set of graphite layer bands for each unit cell. If the band alignments in $KHgC_8$ are similar to that of $KHgC_4$, the main effect of this extra set of bands is to lower the Fermi level. In a simple rigid-band model, lowering the Fermi level of $KHgC_4$ does lower the total density of states, but increases the amalgam contribution until the Fermi level passes below the peak in the partial density of states due to Hg $6p$ contributions.

Fermi-surface extremal orbits for $KHgC_4$ have been measured by the Shubnikov–de Haas technique by Timp *et al.*[7] For two-dimensional Fermi surfaces, the Shubnikov– de Haas frequencies are simply related to the charge associated with each sheet of the Fermi surface.[33] From the very approximate results shown in Fig. 7, the four main sheets of the Fermi surface is expected to result in approximately three Shubnikov–de Haas frequencies. The two types of contributions from the Brillouin-zone corners (from the graphite π bands and from the Hg $6p\sigma$ bands) result in nearly equal extremal areas, each corresponding to approximately 0.25 electrons and a frequency of 2500 T. The hole surface at the zone center due to Hg $6s$ states corresponds to roughly 0.1 electrons and a frequency of 1000 T. The large-electron surface due to Hg $6p\pi$ states would have a frequency of 11 000 T. Except for this high-frequency contribution, these results are remarkably close the results of Timp and coworkers[7] who quote measured frequencies for $KHgC_4$ of 2490, 1090, and 52 T.

Various spectroscopic measurements have been made on samples of $KHgC_4$. X-ray photoemission measurements by DiCenzo *et al.*[1] and electron energy-loss measurements by Preil *et al.*[4] indicate that there is an appreciable amount of K $4s$ character in the occupied states. This is consistent with our results listed in Table II. Since the K $4s$ states strongly hybridize with the valence states of Hg, it is not surprising that the K $4s$ occupation in $KHgC_4$ is greater than in KC_8. Optical reflectivity measurements for $KHgC_4$ by Preil and Fischer[8] indicate that the threshold for interband absorption is 1.3 eV. Although we have we have not attempted to calculate the joint densities of states or optical matrix elements, from the form of the band-structure results in Fig. 6, one expects a substantial contribution to interband absorption at a photon energy of 1.2 eV due to (Hg $6p\pi$)$\rightarrow$(graphite π) band transitions (-1.0 eV$\rightarrow+0.2$ eV) near the Γ-A axis. Our results also indicate that interband transitions at lower photon energies are also possible. In particular, along the Γ-K direction in the Brillouin zone, the weak interaction between the Hg $6p\pi$ and graphite π bands result in a very small band gap near the Fermi level.

In summary, we report the results of self-consistent electronic-structure calculations for $NaHg_2$ and $KHgC_4$. We find that in both of these materials, the Hg $6s$ bands are nearly filled and the Hg $6p$ bands are partially filled. In $KHgC_4$, the amalgam bands are aligned within the manifold of the graphite π bands, resulting in an approximate charge transfer of 0.5 electrons to the graphite π bands and an approximate amalgam carrier charge of 1.5 electrons for each $K_2Hg_2C_8$ unit cell. The charge analysis is very approximate because of its sensitivity to the detailed band shapes beyond the accuracy of calculation. The valence charge density contours show that the Hg layer charge is very similar in $NaHg_2$ and in $KHgC_4$. With the help of a difference density contour plot for $KHgC_4$ we see that the K^+ ions polarize the Hg charge density, the K $4s$ state hybridizing significantly with the Hg $6p\pi$ band. Our results are in qualitative agreement with specific-heat measurements,[9,2,3,32] oscillatory magnetoresistance measurements,[7] and spectroscopic measurements.[1,4,5,8]

ACKNOWLEDGMENTS

This work was supported by the National Science Foundation (NSF), Grant No. DMR-8501022. We would like to thank Professor J. E. Fischer for initiating interest in this project. We would also like to acknowledge the help of Roger brown during the early stages of this project.

[1] S. B. DiCenzo, P. A. Rosenthal, H. J. Kim, and J. E. Fischer, Phys. Rev. B **34**, 3620 (1986).

[2] G. Roth, A. Chaiken, T. Enoki, N. C. Yeh, G. Dresselhaus, and P. M. Tedrow, Phys. Rev. B **32**, 533 (1985).

[3] *Graphite Intercalation Compounds; Progress of Research in Japan,* edited by S. Tanuma and H. Kamimura (World Scientific, Philadelphia, 1985).

[4] M. E. Preil, L. A. Grunes, J. J. Ritsko, and J. E. Fischer, Phys. Rev. B **30**, 5852 (1984).

[5] W. A. Kamitakahara, L. E. DeLong, P. C. Eklund, and R. M. Nicklow, Phys. Rev. B **29**, 490 (1984).

[6] P. Lagrange, M. El Makrini, and A. Herold, Rev. Chem. Miner. **20**, 229 (1983).

[7] G. Timp, T. C. Chieu, P. D. Dresselhaus, and G. Dresselhaus, Phys. Rev. B **29**, 6940 (1984).

[8] M. E. Preil and J. E. Fischer, Solid State Commun. **44**, 357 (1982).

[9] M. G. Alexander, G. P. Goshorn, D. Guerard, P. Lagrange, M. El Makrini, and D. G. Onn, Solid State Commun. **38**, 103 (1981).

[10] L. Senbetu, H. Ikezi, and C. Umrigar, Phys. Rev. B **32**, 750 (1985).

[11] P. Hohenberg and W. Kohn, Phys. Rev. **136**, B864 (1964); W. Kohn and L. J. Sham, *ibid.* **140**, A1133 (1965).

[12]L. Hedin and B. I. Lundqvist, J. Phys. C **4**, 2064 (1971).
[13]S. G. Louie, K.-M. Ho, and M. L. Cohen, Phys. Rev. B **19**, 1774 (1979).
[14]S. G. Louie, S. Froyen, and M. L. Cohen, Phys. Rev. B **26**, 1738 (1982).
[15]G. P. Kerker, J. Phys. C **13**, L189 (1980).
[16]L. Kleinman, Phys. Rev. B **21**, 2630 (1980).
[17]G. B. Bachelet and M. Schluter, Phys. Rev. B **25**, 2103 (1982).
[18]N. A. W. Holzwarth, S. G. Louie, and S. Rabii, Phys. Rev. B **26**, 5382 (1982).
[19]O. Jepsen and O. K. Andersen, Solid State Commun. **9**, 1763 (1971); G. Lehmann and M. Taut, Phys. Status Solidi B **54**, 469 (1972).
[20]G. Gilat and L. J. Raubenheimer, Phys. Rev. **144**, 390 (1966).
[21]G. Gilat and Z. Kam, Phys. Rev. Lett. **14**, 715 (1969).
[22]R. P. Feyman, Phys. Rev. **56**, 340 (1939).
[23]J. W. Nielsen and N. C. Baenziger, Acta Crystallogr. **7**, 277 (1954).
[24]E. J. Duwell and N. C. Baenziger, Acta Crystallogr. **8**, 705 (1955).
[25]The valence pseudodensity accurately represents the actual valence density outside spheres of radii equal to the pseudopotential radii about each atom. Inside the spheres the density has the correct average value but not the correct shape. The pseudopotential radii are chosen so that the outer most peak of the valence wave functions are correctly represented as discussed in Ref. 15.
[26]R. C. Tatar, Ph.D. thesis, University of Pennsylvania, 1985 (unpublished); R. C. Tatar and S. Rabii, in *Extended Abstracts of the Materials Research Society Symposium on Intercalated Graphite,* edited by P. C. Eklund, M. S. Dresselhaus, and G. Dresselhaus (Elsevier, New York, 1984).
[27]D. P. DiVencenzo and S. Rabii, Phys. Rev. B **25**, 4110 (1982).
[28]L. F. Mattheiss and W. W. Warren, Jr., Phys. Rev. B **16**, 624 (1977).
[29]T. Inoshita, K. Nakao, and H. Kamimura, J. Phys. Soc. Jpn. **43**, 1237 (1977); **44**, 689(E) (1977); T. Ohno, K. Nakao, and H. Kamimura, *ibid.* **47**, 1125 (1979).
[30]N. A. W. Holzwarth, S. G. Louie, and S. Rabii, Phys. Rev. B **28**, 1013 (1983).
[31]N. A. W. Holzwarth, D. P. DiVincenzo, R. C. Tatar, and S. Rabii, Int. J. Quantum Chem. **23**, 1223 (1983).
[32]Y. Iye and S. Tanuma, see Ref. 3, p. 256, Phys. Rev. B **25**, 4583 (1982).
[33]N. A. W. Holzwarth, Phys. Rev. B **21**, 3665 (1980).